Region-Based Wavelet Coding Methods for Digital Mammography

Mónica Penedo, William A. Pearlman, Pablo G. Tahoces, Miguel Souto, and Juan J. Vidal

This work was supported in part by the Xunta de Galicia, and Grant TIC2000-0507 from Ministerio de Ciencia y Tecnología (Spain).

M. Penedo is grateful to the Rensselaer Polytechnic Institute for providing residence support during the period this work was done.

M.P., M.S., J.J.V. are from the Department of Radiology, University of Santiago de Compostela, Spain (e-mail: mrmocs@usc.es).

P.G.T. is in the Department of Electronics and Computer Science, University of Santiago de Compostela, Spain.

W.A.P. is in the Department of Electrical, Computer, and Systems Engineering at the Rensselaer Polytechnic Institute, Troy, NY, USA.

Abstract

Spatial resolution and contrast sensitivity requirements for some types of medical image techniques, including mammography, delay the implementation of new digital technologies, namely CAD, PACS or teleradiology. In order to reduce transmission time and storage cost, an efficient data compression scheme to reduce digital data without significant degradation of medical image quality is needed. In this study, we have applied two region-based compression methods to digital mammograms. In both methods, after segmenting the breast region, Region-Based Discrete Wavelet Transform (RBDWT) is applied, followed by an Object-Based extension of the Set Partitioning In Hierarchical Trees (OB-SPIHT) coding algorithm in one method, and an Object-Based extension of the Set Partitioned Embedded bloCK (OB-SPECK) coding algorithm in the other. We have compared these specific implementations against the original SPIHT and the new standard JPEG 2000, both using reversible and irreversible filters, on five digital mammograms compressed at rates ranging from 0.1 to 1.0 bits per pixel (bpp). Distortion was evaluated for all images and compression rates by the Peak Signal-to-Noise Ratio (PSNR). For all images, OB-SPIHT and OB-SPECK performed substantially better than the traditional SPIHT and JPEG 2000, and a slight difference in performance was found between them. A comparison applying SPIHT and the standard JPEG 2000 to the same set of images with the background pixels fixed to zero was also carried out, obtaining similar implementation as region-based methods. For digital mammography, region-based compression methods represent an improvement in compression efficiency from full-image methods, also providing the possibility of encoding multiple regions of interest (ROI) independently.

Keywords

Lossy Image Compression, Region Of Interest (ROI), Region-Based Wavelet Transform, Object-Based Coding, Digital Mammography.

I. Introduction

As new and better methods of digital medical imaging are being developed, digital technology is closer to replacing conventional screen-film imaging. The rapid progress in digital image processing has allowed filtering, enhancement or other types of digital image manipulation that may improve diagnostic interpretation [1], [2]. Digital image format is required in Computer-Aided Diagnosis schemes (CAD) to assist the radiologist in the detection of radiological features that could point to different pathologies [3], [4]. Images in digital format constitute an obligatory requisite towards the implementation of both Picture Archiving and Communications Systems (PACS) and teleradiology.

However, the usefulness of these new techniques mainly depends on two parameters of importance: the spatial and grey-level resolutions. They must provide a diagnostic accuracy in digital images equivalent to that of conventional films. Both pixel size and pixel depth are factors that critically affect the visibility of small-low contrast objects or signals, which often are relevant information for diagnosis [5]. Therefore, digital image recording systems for medical imaging must provide high spatial resolution and high contrast sensitivity.

Nevertheless, this requirement retards the implementation of digital technologies due to the increment in processing and transmission time, storage capacity and cost that good digital image quality implies. For instance, it has been shown that isolated clusters of microcalcifications are one of the most frequent radiological features of asymptomatic breast cancer. A careful search for the clustered microcalcifications that may herald an early-stage cancer should be done on all mammograms [6]. Microcalcifications frequently appear as small size, low contrast radiopacities [7]. Because of this, a typical mammogram must be digitized at a resolution of about 4000 x 5000 pixels with 50 μm spot size and 12 bits, resulting in approximately 40Mb of digital data. Processing or transmission time of such digital images could be quite long. Also, archiving the amount of data generated in any screening mammography program becomes an expensive and difficult challenge.

It is clear that advances in technologies for transmission or storage are not sufficient to solve this problem. An efficient data compression scheme to reduce the digital data without significant degradation of the medical image quality for human and machine interpretation is needed. Several lossless (with exact reconstruction of the original image after compression) and lossy (some information is lost in the compression process) compression methods have been investigated for medical imaging applications [8]-[10]. However, lossless techniques provide only modest reduction in file size. To significantly affect transmission and storage costs, lossy compression methods are required, always taking into consideration that the loss must not be diagnostically significant for the specific clinical issue to be addressed. Receiver Operating Characteristic (ROC) analysis on lossy compression showed that it is possible to use lossy techniques in medical image compression, provided that the diagnostic power is not lost or diminished [11]-[14].

Previously research works have evaluated, with CAD systems or observer's performance studies, lossy compression in digital mammography. Perlmutter et al. evaluated fifty-seven digital mammograms compressed with the Set Partitioning In Hierarchical Trees (SPIHT) algorithm [15]. They found no significant differences between analog and compressed images even at the lowest bit rate tested, 0.15 bpp (80:1 compression ratio). Good et al. assessed the detection of masses and clustered microcalcifications, by means of an ROC study, in sixty digital mammograms compressed using the old standard JPEG (Joint Photographic Experts Group) [13]. Their results showed that detection of masses is not affected by compression while observer performance is degraded for detecting clusters of microcalcifications at ratios of 101:1. In a similar study, Zheng et al. compared the performance of a CAD system for the detection of primary signs of breast cancer using original images and images reconstructed after JPEG compression [14]. They obtained that JPEG does not affect the CAD scheme for detecting masses, but detection of cluster of microcalcifications is affected with compression. In all these research studies, optimization of the compression process is obtained identifying the least rectangular area containing the breast region and compressing it at a different factor than the rest of the image.

Encoding of arbitrarily shaped regions inside an image at different quality levels can help to develop medical image compression methods that focus on those regions that are important for diagnostic purposes. Generally, in region of interest (ROI) coding the whole image is transformed and those coefficients associated to the ROI are coded at higher precision (up to lossless) than the background. After segmenting the image into important regions (automatically or manually), coding of only ROI related coefficients can be accomplished either after a certain compression bit rate of the entire image has been reached [16], or before the information associated to the background [17], as in the JPEG 2000 standard [18],[19].

The Maxshift method, described in the JPEG 2000 Part 1 for ROI coding [20], scales wavelet coefficients inside the region area by a scaling factor 2^s, where s is the highest non-allzero bit plane in the magnitudes of the wavelet transform coefficients formed solely from background pixels. A binary shape mask is formed for the wavelet transform corresponding to the image domain ROI. This mask will contain more coefficients than pixels in the image ROI, because filtering beyond the region of interest in the image can involve pixels within the boundary. This shape information need not be sent to the decoder, because, after decoding, the only wavelet coefficients with magnitudes greater than 2^s belong to the transform ROI. These coefficients are then scaled down by 2^s prior to inverting the transformation to produce the reconstructed image. Since wavelet coefficients corresponding to the image ROI boundary are formed from pixels both inside and outside the boundary, encoding distortion in ROI wavelet coefficients may propagate outside the image ROI boundary and vice-versa. Although the Maxshift method is compatible with an arbitrary region shape, software implementations of JPEG2000 Part I allow only rectangular or circular shapes.

Using a general scaling-based method, as it is described in Part 2 extension of the JPEG 2000 standard [18],[19], ROI coefficients can be scaled using an arbitrary value allowing to determine different regions at different quality. Transmission of ROI shape information is needed with this general method.

The growing interest in manipulating visual objects in digital images or video has led to new region-based (or contour-texture) coding techniques, which describe the images in terms of arbitrary contours and textures (pixels inside the contour) that are coded separately [21],[22]. These new techniques apply shape-adaptive transformation only to the pixels inside the object to be encoded. In a shape-adaptive wavelet transform, an arbitrary ROI is represented by the same number of coefficients in the transform domain as samples within the region in the image domain. Maxshift or scaling-based methods need to encode more coefficients than pixels in the image ROI. As in the general scaling-based method, object shape information needs to be transmitted.

In this study, we have implemented two region-based coding methods for digital mammography. These methods are adaptations of the work of Z. Lu in object-based video coding [23],[24]. In both methods, a border detection technique segmented the mammogram into the tissue area and the radiological background. Then, as part of the texture coding method, a Region-

Based Discrete Wavelet Transform (RBDWT) was applied to the tissue area to decompose the arbitrary region into wavelet subbands [25],[26]. In one of the methods implemented, an Object-Based extension of the Set Partitioning In Hierarchical Trees (OB-SPIHT) algorithm [27] was used to encode the wavelet coefficients. For the second method, an Object-Based extension of the Set Partitioned Embedded bloCK (OB-SPECK) coder was used [28]. SPIHT and SPECK are state-of-the-art image compression techniques having the characteristics of low complexity and embedded (progressive) bit streams. These region-based techniques, described in detail in Section II, have been compared in mammographic images to SPIHT and the new standard JPEG 2000 when compressing the full original image and the image with the background previously set to zero. The former quantifies the performance improvement of object-based over full-image techniques; the latter is a comparison to a candidate region-based technique. Section III presents the results of the quantitative measurements obtained. Advantages and disadvantages of the various techniques are discussed in Section IV.

II. Material and Methods

A. Digital Images

Five single-view conventional mammograms containing clusters of microcalcifications and masses, all biopsy proven, were used in this study. The images had been collected over a period of time from the daily clinical case load in the Department of Radiology of the Hospital Xeral de Galicia, University of Santiago de Compostela (Spain). Mammograms were digitized with a commercially available LUMISCAN 85 laser film digitizer Lumisys INC., resulting in images of 4096 x 5120 pixels at 12 bits.

B. Mammogram Segmentation

In a typical digitized mammogram much of the area in the image corresponds to background pixels rather than to tissue pixels. To optimize compression in digital mammograms it is important to code the least information about background as possible. Detection of the breast border allows segmentation of the image for compression of the breast region only. The automatic method used for detecting the breast border was described in detail in [29]. Briefly, first a thresholding is applied to improve the performance of the detection method: two cut-off gray levels are used to threshold the image in order to eliminate artifacts and get an homogeneous background. Then, a smoothed version of the thresholded image is generated. Five reference points, (x_1, y_1), (x_2, y_2), (x_3, y_3), (x_4, y_4), and (x_5, y_5), are automatically selected dividing the breast into three regions (Fig. 1).

Finally a tracking algorithm detects the border establishing that a point (x_i, y_i) belongs to the breast border if the gray level value, $f(x, y)$, of its nine previous pixels verify the condition: $f(x_{i-9}, y_{i-9}) < f(x_{i-8}, y_{i-8}) < \ldots < f(x_{i-3}, y_{i-3}) \leq f(x_{i-2}, y_{i-2}) \leq f(x_{i-1}, y_{i-1}) \leq f(x_i, y_i)$ The tracking process is applied along different directions depending on the breast region. In region I the algorithm searches the breast border from left to right; in region II from top to bottom; and finally in region III the border is searched from right to left (Fig. 1). The detection algorithm was relaxed such that the breast border obtained was always external to the real border.

Calculating the slope of the breast border in the reference points (x_1, y_1) and (x_2, y_2), the detected border was enlarged until it reached the edge of the digital image. Hence, the breast region where the relevant information for diagnosis is included was completely determined within a closed contour (Fig. 1). Then, a binary mask is constructed with the object shape information determined. This mask will be used in the Contour Coding and Region-Based Wavelet Transform processes.

C. Contour Coding

In region-based coding methods, the object shape information has to be coded before the texture of the object. Shape coding methods may be lossless or lossy methods. According to the coding technique, shape coding methods are classified into block-based or contour-based techniques. In the first, the binary image representing the object shape is encoded as in a conventional image coding method. In the latter, the information coding is performed along the object edge in the binary mask.

Among the contour-based techniques, a chain code [30] is one of the most frequently used methods for lossless coding of the object shape information. In this method, instead of encoding the absolute position of each contour point, the relative position between two consecutive points, called a *link*, is encoded. Therefore, an initial point in the contour object and the necessary links following this point to describe the object shape are enough for reconstructing the object shape.

To improve the coding efficiency of the chain code method, a large number of schemes are proposed by imposing certain conditions on the contour or by exploiting the spatial characteristic of the contour [31]-[33]. In this implementation, a two-link chain coding method presented in [23], [34] is applied for coding the breast border.

D. Region-Based Discrete Wavelet Transform

The Region-Based Discrete Wavelet Transform (RBDWT) we have used for coding the texture was proposed by Barnard in [25]. Using RBDWT it is possible to efficiently perform wavelet subband decomposition of a region of arbitrary shape, while maintaining the same number of wavelet coefficients to be coded than pixels within the region and keeping spatial correlation and self-similarity across subbands [25],[26].

The binary mask obtained during the segmentation process will specify the breast region inside the image where the RBDWT will be applied to obtain the first wavelet decomposition level of the image. In order to get the next decomposition level, it will be necessary to identify which wavelet coefficients in the LL subband determine the area where the RBDWT must be applied again. This information is provided decomposing the binary mask analogously to the wavelet subband decomposition of the image (Fig. 2). The LL subimage of the decomposed binary mask specifies the region in the LL wavelet subband of the decomposed image where the RBDWT will be applied again. Decomposition of the binary mask will continue on the LL subimage to get the next wavelet decomposition level of the breast region, continuing this process until the required image decomposition level.

Using separable wavelet filters, the 2D RBDWT is achieved applying 1D arbitrary length signal transform by rows and then by columns on the pixels inside the image object. Efficient signal extensions allow decomposition up to an arbitrary level for arbitrary length signals with perfect reconstruction property and without increasing the total number of samples, i.e. if the original signal has length N, the same number of wavelet coefficients will represent the signal after transformation [25].

The 1D signal segments inside the arbitrary shape do not all start at an even- or odd-numbered position inside the row or column. Therefore, a proper subsampling strategy in the filter process has to be chosen in order to preserve the spatial correlation within the image object. Depending on the parity of the segment length and the parity of the position at which the segment starts in the row or column, there are four classes of 1D signal segments inside the object, which require different signal extension and subsampling [25].

A 5-level dyadic decomposition of the breast region inside the mammogram was obtained with the 2D RBDWT method using 9-tap/7-tap biorthogonal filters [35].

E. Coding of the Wavelet Coefficients

SPIHT (Set Partitioning In Hierarchical Trees) and SPECK (Set Partitioned Embedded bloCK) are both efficient wavelet-based codecs, which represent the state of the art in image compression performance. The SPIHT image codec was developed by Said and Pearlman [27] and the SPECK codec by Islam and Pearlman [28]. The SPIHT technique is an extension and improvement over the Embedded Zerotree Wavelets (EZW) algorithm developed by Shapiro [36], and it has been applied successfully in lossy compression of medical images [12],[15].

Both algorithms are embedded techniques, i.e. the coding method produces an embedded bitstream which can be truncated at any point, equivalent to stopping the compression process at a desired rate, whereupon the image can be reconstructed. The wavelet coefficients with larger magnitude are those with a larger content of information. An embedded method transmits first those coefficients in order to achieve a reconstructed image with the minimum distortion for a given compression rate. The SPIHT and SPECK algorithms order the wavelet coefficients according to its binary representation and transmit first an approximation of the most important coefficients providing a progressive in fidelity method based on a bitplane transmission where coefficients are progressively refined.

The partial ordering by magnitude of the transformed coefficients $c(i,j)$ is due to sequential comparisons of coefficient magnitudes to a set of decreasing thresholds 2^{n_o-1}, 2^{n_o-2}, ..., with the initial threshold 2^{n_o} satisfying the condition $2^{n_o} \leq \mid c(i,j) \mid < 2^{n_o+1}, \forall c(i,j)$. Coefficients with magnitudes equal or larger than the considered threshold, 2^n, $n < n_o$, are classified as *significant*, while others are classified as *insignificant*.

In order to reduce the number of comparisons, the procedure called the *sorting pass* divides the set of pixels into partitioned subsets T_m and performs the magnitude test,

$$max_{(i,j)\in T_m}\{c(i,j)\} \geq 2^n, \tag{1}$$

for each. If the subset is *significant*, then a fixed rule is used to partition T_m into new subsets where the magnitude test is applied again. If the subset is *insignificant*, all coefficients in T_m

are insignificant, so that sorting stops for this subset at threshold 2^n. The test in Equation (1) is called a *significance* test.

The specific initial sets and partitioning rules are different for SPIHT and SPECK. While the former exploits the spatial self-similarity across subbands inherent in the wavelet decomposition of natural images [37], the latter takes advantage of the clustering of energy in frequency and space in hierarchical structures of transformed images. SPIHT organizes wavelet coefficients belonging to similar spatial orientation into trees, spanning subbands from the lowest spatial frequency at the root to the highest frequency subbands at the leaves, as shown in Fig.3(a). When a set of descendants of a node in the tree is significant, it is divided into the four isolated offspring coefficients and all the descendants of the offspring. SPECK employs two recursive partitioning procedures upon the wavelet coefficients in order to test significance and encode rectangular blocks of varying dimensions, called sets of type I or S. Figure 3(b) illustrates the octave band partitioning of a significant set I into three S sets, each comprising a whole subband, and a new I. Such partitioning is applied recursively to generate S sets that increase in size by octaves until the last I set in the lower right corner becomes identical to the S set comprising the highest spatial frequency subband. Figure 3(b) also shows the quadrisection of a significant S set into four offspring sets $O(S)$. This procedure is applied recursively until the significant pixels are located. Both SPIHT and SPECK output sequences of significance test bits, called a *significance map*, that may be associated with the construction of quadtrees.

E.1 Object-Based extensions of SPIHT and SPECK

The binary mask obtained during the segmentation process provides the shape information needed for extending the conventional SPIHT and SPECK algorithms. With the pyramidal shape mask constructed as it has been explained in section D (Fig. 2), the nodes belonging to the breast region in each subband are known.

Figures 4 and 5 show how the set partitioning produces branches to subsets falling outside the object. In the object-based extensions, before the coding process, the nodes and child branches outside the image object are pruned. During the coding process, no information about nodes and branches outside the breast region needs to be transmitted [23],[24].

F. Numerical quality evaluation

Lossy compression performance of the two proposed region-based wavelet coding methods was evaluated at different rates on a set of five digital mammograms. The coding results were compared with those obtained applying the original SPIHT algorithm and the standard JPEG 2000 [20] on the whole image. The SPIHT algorithm has been utilized with the irreversible 9/7 biorthogonal filters [35] and with the reversible S+P filter [38] to examine lossy to lossless coding. Similarly, JPEG 2000 has been applied using the 5/3 reversible and the 9/7 irreversible filters. OB-SPIHT and OB-SPECK were also compared to SPIHT and JPEG 2000 applied to the same set of images with the background previously fixed to a constant value of zero. With these pre-processed images, both algorithms encode the breast region before the background pixels resulting, for this study, in similar implementations to that of region-based methods.

The reconstruction quality of all methods was evaluated by means of the Peak Signal-to-Noise Ratio (PSNR)

$$PSNR = 10\log_{10}\left(\frac{4095^2}{MSE}\right) \quad dB$$

where 4095 is the peak amplitude and MSE is the mean squared-error between the original and the reconstructed image. In order to compare region-based methods to one another and to full-image coding, the MSE measurements for all methods were calculated for each image only within the same breast region where the object-based coding methods were applied.

In all the SPIHT and SPECK full-image or object-based methods, reported decompression results were obtained from the same associated compressed file coded to 1.0 bit per pixel or higher. However, for JPEG 2000 reported results were obtained from compressed files encoded and decoded to the same bit rate using Verification Model Version 8.5 (VM8.5)[39]. All bit rates were calculated from the actual size of the compressed file.

III. Results

Tables I-V summarize the coding results obtained at rates ranging from 0.1 to 1.0 bpp for each digital mammogram. For all images, the region-based transform/coding methods, OB-SPIHT and OB-SPECK, performed substantially better than normal SPIHT and JPEG2000 applied to the whole image, with irreversible and reversible filters.

OB-SPECK showed a very slight PSNR advantage over OB-SPIHT. The SPIHT and JPEG-2000 methods applied to the images with background set to zero, which we call SPIHTroi and

JP2Kroi, proved to be quite competitive in PSNR with the two object-based coding methods applied to the mammogram region. Note the high PSNR values of 56 to 80 dB obtained with SPIHTroi, JP2Kroi, and region-based methods at 1.0 bit per pixel. As a point of reference, the average lossless rate achieved with SPIHT S+P and JPEG 2000 5/3 was, respectively, 5.90 bpp and 5.99 bpp, so there are still substantial savings in file size achievable with lossy methods.

In figure 6 comparative results between OB-SPIHT and OB-SPECK with SPIHT and JPEG 2000 are shown for mammogram h60ci, which presents the lowest difference in performance between region-based and full-image methods. Yet, even with this image, a remarkable improvement on distortion measurements was found for the object-based techniques compared to JPEG 2000 and to SPIHT. On average, for h60ci, object-based techniques improve, respectively, general SPIHT and JPEG 2000 by 0.920 dB and 0.710 dB at 0.1 bpp, and by 5.035 dB and 4.550 dB at 1.0 bpp, the highest rate tested. Figure 7 plots the PSNR measurements for image h56cd, which achieves one of the highest differences in performance between region-based methods and SPIHT and JPEG 2000. In fact, the distortion achieved at around 1.0 bpp with SPIHT or the standard JPEG 2000 method corresponds to a compression rate of 0.2 bpp with OB-SPIHT and OB-SPECK, making clear the improvement obtained with the object-based compression techniques.

For all images, the climb of PSNR versus rate for full-image SPIHT and JPEG 2000 is quite slow and even flat for some images in some ranges of rate, whereas this climb is, on average, an almost constant 4 dB per 0.2 bpp for the object-based techniques. The full-image wavelet transform blends the black pixels of the background and the nearly white pixels of the object in the region embracing the boundary, making the resulting coefficients within the object region harder to encode efficiently.

Tables and graphs show that SPIHTroi and JP2Kroi produce almost the same PSNRs in the breast region as OB-SPECK and OB-SPIHT. Actually, on average, object-based methods always introduced less distortion than SPIHTroi, but JP2Kroi was sometimes slightly better than all of them.

Reconstructed images obtained after compression at 0.4 bpp with a full-image (SPIHT) and an object-based (OB-SPIHT) method compared in this study are shown in Figure 8. SPIHT and JPEG 2000 compress the whole image; thus, information from background is included in the reconstruction image. However, OB-SPIHT and OB-SPECK improve in efficiency compressing only the breast region inside the mammogram and discarding the radiological background, which has no diagnostic interest. The regions of interest marked in Figure 8 are magnified in Figure 9. Although the reconstructed ROIs are at the same rate, more rice artifacts are visible in the SPIHT and JPEG2000 methods compared to region-based methods and JP2Kroi (Fig. 9).

IV. Discussion and Conclusion

Region of interest (ROI) coding techniques are particularly suitable for medical imaging. Such methods provide the possibility of adequately compressing those regions with diagnostic relevance with better quality than the rest of the image. OB-SPIHT and OB-SPECK are object-based extensions of full-image SPIHT and SPECK algorithms, which represent the state of the art in image compression. Both techniques preserve the features of the original methods, providing progressive transmission of images, gradually improving the image quality. The encoding/decoding algorithms can even be let run until the reconstructed image is a nearly lossless representation of the original one. These features make these compression methods appropriate for telemammography, allowing to transmit a first approximation of the original digitized mammogram and progressively increase the pixel accuracy until a radiologist could diagnose with the reconstructed image quality achieved.

Preceding studies applying irreversible compression methods to digital mammography determined that loss of information does not affect diagnostic interpretation when compression rates are limited to certain ranges [13]-[15]. However, in these research works compression has been applied to the least rectangular area containing the breast region. In our work, we have adapted OB-SPIHT and OB-SPECK to digital mammography coding only the breast region, where the important information is included.

We have shown that OB-SPIHT and OB-SPECK exhibit much higher quality in the breast region at the same compressed file size than full-image compression methods as SPIHT and the standard JPEG 2000. It has also been shown that SPIHTroi and JP2Kroi, both analogous to scaling-based compression methods, are competitive in PSNR to OB-SPIHT and OB-SPECK. Therefore, an improvement in compression efficiency in digital mammography can be expected for ROI-based methods compared to full-image methods where the compressed file contains information beyond the breast region.

Object or region-based compression methods transform only those pixels within the ROI and the same number of wavelet coefficients are coded. In the scaling-based methods supported in the standard JPEG 2000, where the wavelet transform is applied to the entire image, more coefficients than pixels within the ROI are necessary to obtain perfect reconstruction of the region. A more efficient coding of the ROI is then expected with object-based methods but at the expense of an increment in computational cost associated to the region-based wavelet transform compared to the conventional transform. On the other hand, region-based and general scaling-based methods need to encode the shape information of the ROI meanwhile this is not necessary with the Maxshift method, resulting in a coding efficiency increment.

Certain applications would benefit from the possibility of determining several regions with different importance within an image before compression. For example, regions inside the mammogram containing primary radiological signs of breast cancer, such as clusters of microcalcifications and masses, can be determined by an expert radiologist or a CAD system as a preliminary step in a compression scheme for digital mammography. These areas can be compressed at a different ratio than the rest of the breast and, furthermore, the radiological background can be discarded. Encoding techniques, such as OB-SPIHT and OB-SPECK, permit the compression of multiple regions with precise bit rate control yielding different quality levels within the image. The feature of multiple quality levels is also provided in the general scaling-based method of the ROI coding mode supported in the JPEG 2000, but it is not permitted in the Maxshift method [19]. In scaling-based methods, control of bit rate in ROI regions, although supported, but not specified in JPEG 2000, would be inordinately cumbersome to implement. The standard has also avoided the overhead associated with the encoding of the shape information defining only rectangular and ellipse regions, although principles of the general scaling-based method can be extended to handle regions with arbitrary shape. However, a scaling coefficients procedure, especially in multiple regions, may require downward scaling of the background due to precision limitations. In that case, the least significant bitplanes are lost, causing additional quality degradation of the background [18].

Motivated by the results obtained in this work, our next study will carry out the clinical evaluation of these region-based wavelet coding techniques in digital mammography.

References

[1] P. G. Tahoces, J. Correa, M. Souto, C. González, L. Gómez, and J. J. Vidal, "Enhancement of chest and breast radiographs by automatic spatial filtering," *IEEE Trans. Med. Imag.*, vol. 10, pp. 330-335, Sep. 1991.

[2] M. Souto, J. Correa, P. G. Tahoces, D. Tucker, K. S. Malagari, J. J. Vidal, and R. G. Fraser, "Enhancement of chest images by automatic adaptive spatial filtering," *J. Digit. Imaging* , vol. 5, pp. 223-229, Nov. 1992.

[3] A. J. Méndez, P. G. Tahoces, M. J. Lado, M. Souto, and J. J. Vidal, "Computer-aided diagnosis: Automatic detection of malignant masses in digitized mammograms," *Med. Phys.*, vol. 25, pp. 957-964, June 1998.

[4] M. J. Lado, P. G. Tahoces, A. J. Méndez, M. Souto, and J. J. Vidal, "Evaluation of an automated wavelet-based system dedicated to the detection of clustered microcalcifications in digital mammograms," *Med. Inform.Internet Med.*, vol. 26, pp. 149-163, July 2001.

[5] H-P. Chan, L. T. Niklason, D. M. Ikeda, K. L. Lam, and D. D. Adler, "Digitization requirements in mammography: Effects on computer-aided detection of microcalcifications," *Med. Phys.*, vol. 21, pp. 1203-1211, July 1994.

[6] D. B. Kopans, *Breast imaging*, 2nd ed., Philadelphia, PA: Lippincott-Raven Publishers, 1998.

[7] R. E. Bird, T. W. Wallace, and B. C. Yankaskas, "Analysis of cancer missed at screening mammography," *Radiology*, vol. 184, pp. 613-617, Sep. 1992.

[8] G. R. Kuduvalli and R. M. Rangayyan, "Performance analysis of reversible image compression techniques for high-resolution digital teleradiology," *IEEE Trans. Med. Imag.*, vol. 11, pp. 430-445, Sep. 1992.

[9] H-P. Chan, S-C. B. Lo, L. T. Niklason, D. M. Ikeda, and K. L. Lam, "Image compression in digital mammography: Effects on computerized detection of subbtle microcalcifications," *Med. Phys.*, vol. 23, pp. 1325-1336, Aug. 1996.

[10] G. S. Maitz, T. S. Chang, J. H. Sumkin, P. W. Wintz, C. M. Johns, M. Ganott, B. L. Holbert, C. M. Hakim, K. M. Harris, D. Gur, and J. M. Herron, "Preliminary clinical evaluation of high-resolution telemammography system," *Invest. Radiol.*, vol. 32, pp. 236-240, 1997.

[11] H. MacMahon, K. Doi, S. Sanada, S. M. Montner, M. L. Giger, C. E. Metz, N. Nakamori, F-F. Yin, X-W. Xu, H. Yonekawa, and H. Takeuchi, "Data compression: Effect on diagnostic accuracy in digital chest radiography," *Radiology*, vol. 178, pp. 175-179, Jan. 1991.

[12] V. Savcenko, B. J. Erickson, P. M. Palisson, K. R. Person, A. Manduca, T. E. Hartman, G. F. Harms, and L. R. Brown, "Detection of subtle abnormalities on chest radiographs after irreversible compression," *Radiology*, vol. 206, pp. 609-616, March 1998.

[13] W. F. Good, J. H. Sumkin, M. Ganott, L. Hardesty, B. Holbert, C. M. Johns, and A. H. Klym, "Detection of masses and clustered microcalcifications of data compresed mammograms: An observer performance study," *Am. J. Roent.*, vol. 175, pp. 1573-1576, Dec. 2000.

[14] B. Zheng, J. H. Sumkin, W. F. Good, G. S. Maitz, Y.-H. Chan, and D. Gur, "Applying computer-assisted detection schemes to digitized mammograms after JPEG data compression: an assessment," *Acad. Radiol.* vol. 7, pp. 595-602, Aug. 2000.

[15] S. M. Perlmutter, P. C. Cosman, R. M. Gray, R. A. Olshen, D. Ikeda, C. N. Adams, B. J. Betts, M. B. Williams, K. O. Perlmutter, J. Li, A. Aiyer, L. Fajardo, R. Birdwell, and B. L. Daniel, "Image quality in lossy compressed digital mammograms," *Signal Processing*, vol. 59, pp. 189-210, June 1997.

[16] A. Järvi, J. Lehtinen, and O. Nevalainen, "Varible quality image compression system based on SPIHT," *Signal Process.: Image Comm.* vol. 14, pp. 683-696, July 1999.

[17] E. Atsumi and N. Farvadin, "Lossy/lossless region-of-interest image coding based on the set partitioning in hierarchical trees," *Proc. IEEE Int. Conf. Image Processing (ICIP)* vol. 1, pp. 87-91 1998.

[18] C. Christopoulos, J. Askelöf, and M. Larsson, "Efficient methods for encoding regions of interest in the upcoming JPEG2000 still image coding standard," *IEEE Signal Processing Lett.* vol.7, pp. 247-249, Sep. 2000.

[19] M. Rabbani and R. Joshi, "An overview of the JPEG 2000 still image compression standard," *Signal Process.: Image Comm.* vol. 17, pp. 3-48, Jan. 2002.

[20] J. Askelöf, M. L. Carlander, and C. Christopoulos, "Regions of interest coding in JPEG 2000," *Signal Process.: Image Comm.* vol. 17, pp. 105-111, Jan. 2002.

[21] M. Kunt, A. Ikonomopoulos, and M. Kocher, "Second generation image coding techniques," in *Proc. IEEE*, vol. 73, pp. 549-575, April 1985.

[22] G. Minami, Z. Xiong, A. Wang, and S. Mehrotra, "3-D wavelet coding of video with arbitrary regions of support," *IEEE Trans. Circuits Syst. Video Technol.* vol. 11, pp. 1063-1068, Sep. 2001.

[23] Z. Lu, "New coding systems for wavelet transforms of signals," Ph.D. dissertation, Rensselaer Polytechnic Institute, Troy, New York, USA, 2000.

[24] Z. Lu and W. A. Pearlman, "Wavelet Video Coding of Video Object by Object-based SPECK Algorithm," *Picture Coding Symposium (PCS 2001)*, pp. 413-416, April 2001.

[25] H. J. Barnard, "Image and video coding using a wavelet decomposition," Ph.D. dissertation, Delf University of Technology, Delf, The Netherlands, 1996.

[26] S. Li and W. Li, "Shape-adaptive discrete wavelet transform for arbitrarily shaped visual object coding," *IEEE Trans. Circuits Syst. Video Technol.*, vol. 10, pp. 725-743, Aug. 2000.

[27] A. Said and W. A. Pearlman, "A new fast and efficient image codec based on set partitioning in hierarchical trees," *IEEE Trans. Circuits Syst. Video Technol.*, vol. 6, pp. 243-250, June 1996.

[28] A. Islam and W. A. Pearlman, "An embedded and efficient low-complexity hierarchical image coder," in *Proc. SPIE Visual Comm. and Image Processing*, vol. 3653, pp. 294-305, 1999.

[29] A. J. Méndez, P. G. Tahoces, M. J. Lado, M. Souto, J. Correa, and J. J. Vidal, "Automatic detection of breast border and nipple in digital mammograms," *Comput. Methods Programs Biomed.*, vol. 49, pp. 253-262, May 1996.

[30] H. Freeman, "On the encoding of arbitrary geometric configurations," *IRE Trans. Electronic Computers*, vol. 10, pp. 260-268, 1961.

[31] T. Kaneko and M. Okudaira, "Encoding of arbitrary curves based on the chain code representation," *IEEE Trans. Commun.*, vol. 33, pp. 697-707, July 1985.

[32] L. Labelle, D. Lauzon, J. Konrad, and E. Dubois, "Arithmetic coding of a lossless contour-based representation of label images," in *IEEE Int. Conf. Image Processing (ICIP)*, vol. 1, pp. 261-265, 1998.

[33] M. Eden and M. Kocher, "On the performance of a contour coding algorithm in the context of image coding. Part I: Contour segment coding," *Signal Processing*, vol. 8, pp. 381-386, July 1985.

[34] Z. Lu and W. A. Pearlman, "Motion Compensated Two-link Chain Coding for Binary Shape Sequences," *Visual Communications and Image Processing 2002*, Proceedings of SPIE, Vol. 4671, pp. 356-362, Jan. 2002.

[35] M. Antonini, M. Barlaud, P. Mathieu, and I. Daubechies, "Image coding using wavelet transform," *IEEE Trans. Image Processing*, vol. 1, pp. 205-220, Apr. 1992.

[36] J. M. Shapiro, "Embedded image coding using zerotrees of wavelet coefficients," *IEEE Trans. Signal Processing*, vol. 41, pp. 3445-3462, Dec. 1993.

[37] A. S. Lewis and G. Knowles, "Image compression using the 2-D wavelet transform," *IEEE Trans. Image Processing*, vol. 1, pp. 244-250, Apr. 1992.

[38] A. Said and W. A. Pearlman, "An Image Multiresolution Representaion for Lossless and Lossy Compression," *IEEE Trans. Image Processing*, vol. 5, pp. 1303-1310, Sep. 1996.

[39] JPEG 2000, Verification Model Software 8.5, ISO/IEC JTC1/SC29/WG1 N1894, 2000.

List of Figures

List of Tables

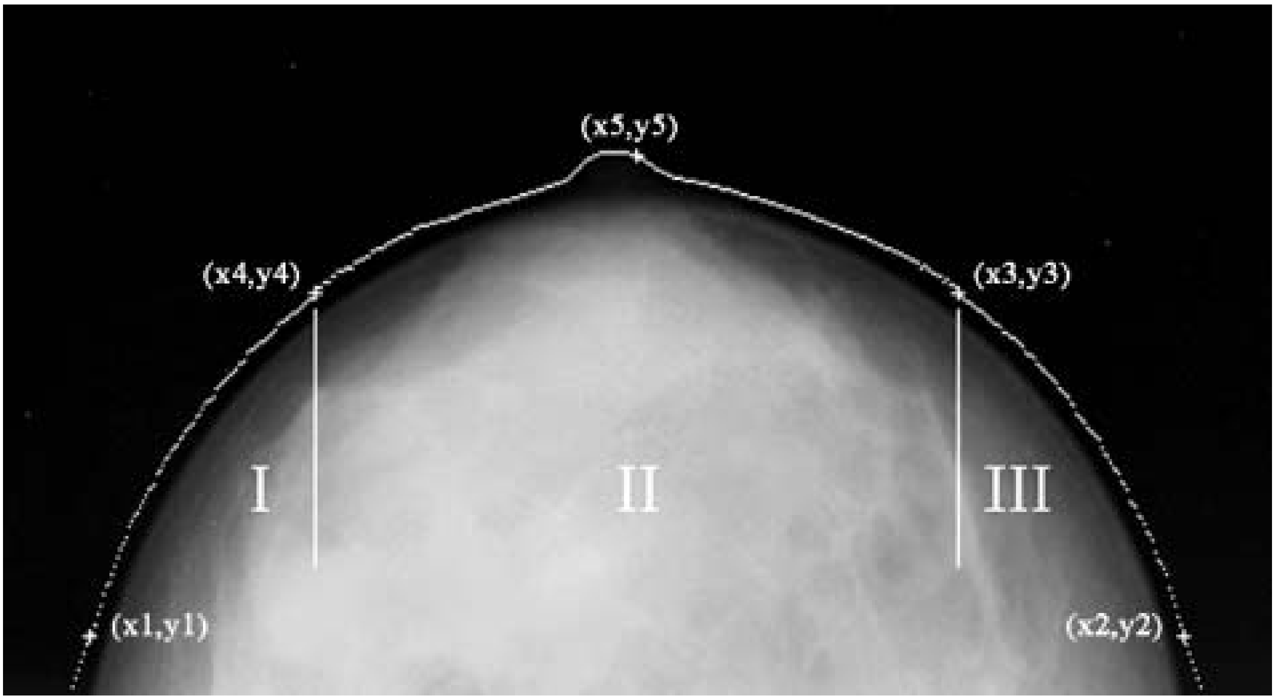

Fig. 1. Closed contour determined in the segmentation process. Reference points dividing the breast into three regions are also shown.

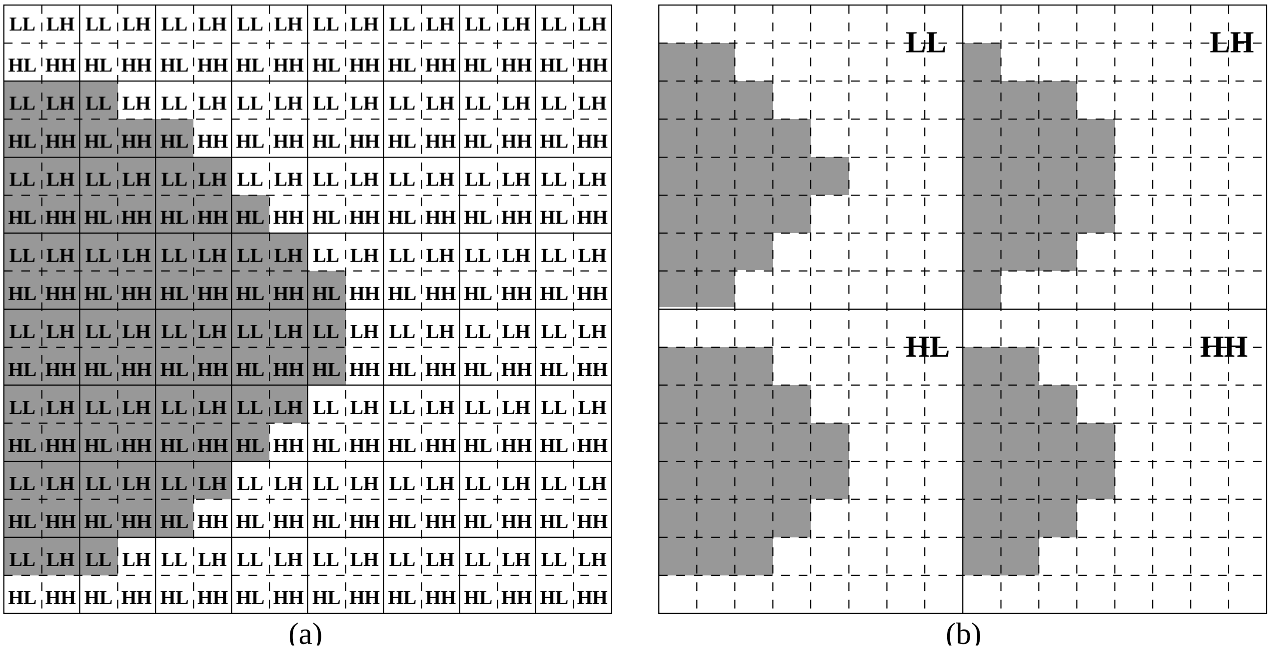

Fig. 2. Decomposition of the binary mask: (a) the original binary mask is divided in blocks of 2x2 pixels; each pixel in the block corresponds to a subband, (b) splitting the original mask into four subimages.

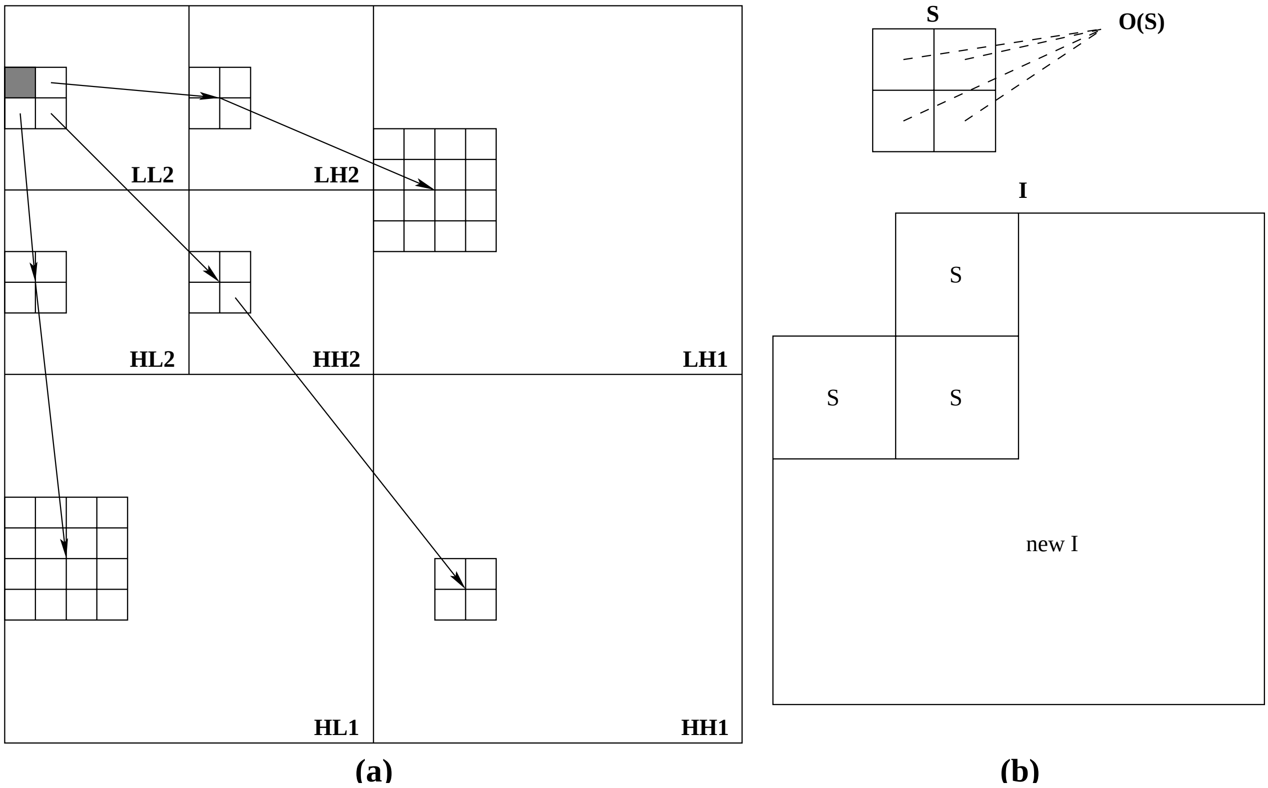

Fig. 3. (a) Spatial Orientation Tree showing dependencies between coefficients in different subbands in SPIHT coding algorithm; (b) Set Partitioning rules for SPECK algorithm. Top: Quadtree Partitioning rule for set S. Bottom: Octave Band Partitioning rule for set I .

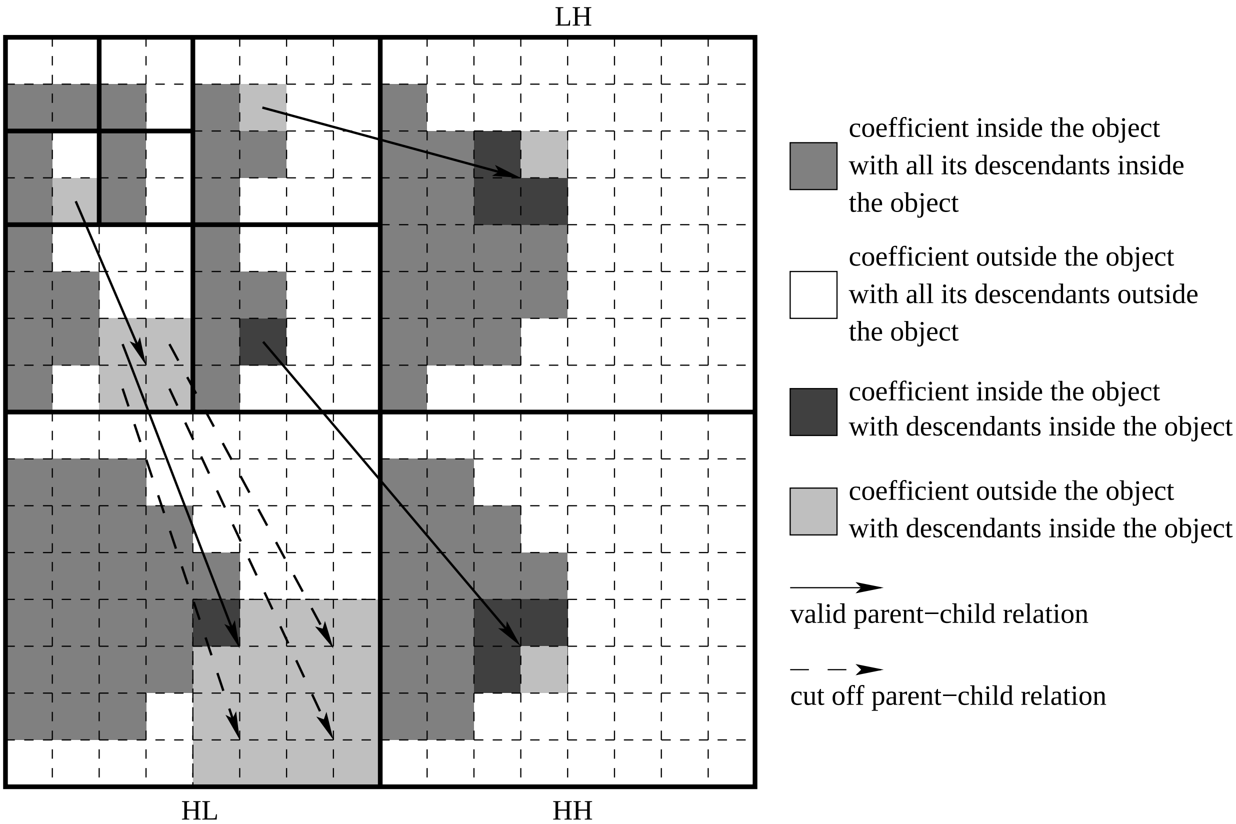

Fig. 4. Parent-child relations in the OB-SPIHT algorithm.

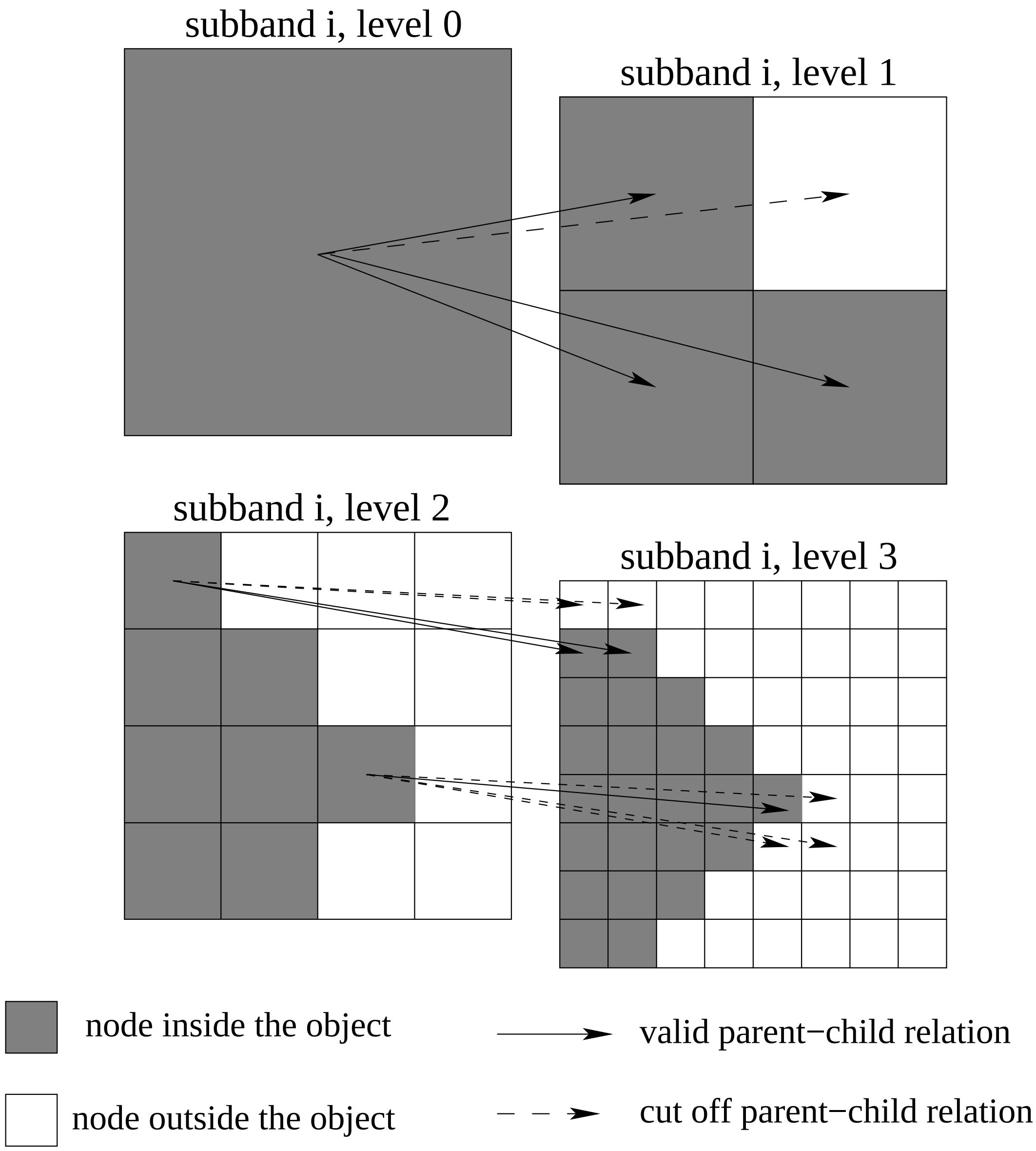

Fig. 5. Parent-child relations in the OB-SPECK algorithm.

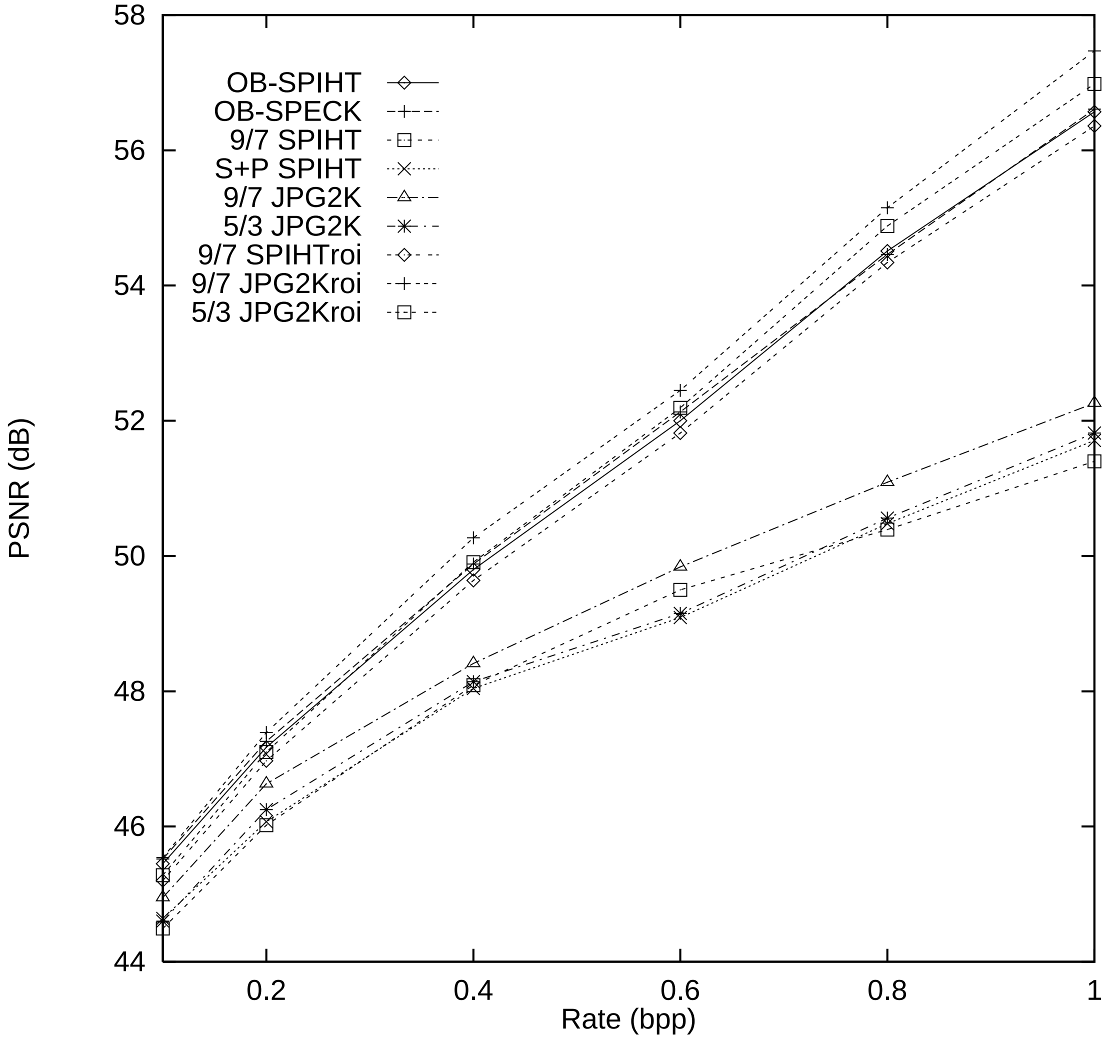

Fig. 6. Comparative evaluation of OB-SPIHT and OB-SPECK with SPIHT and JPEG 2000 for mammogram h60ci.

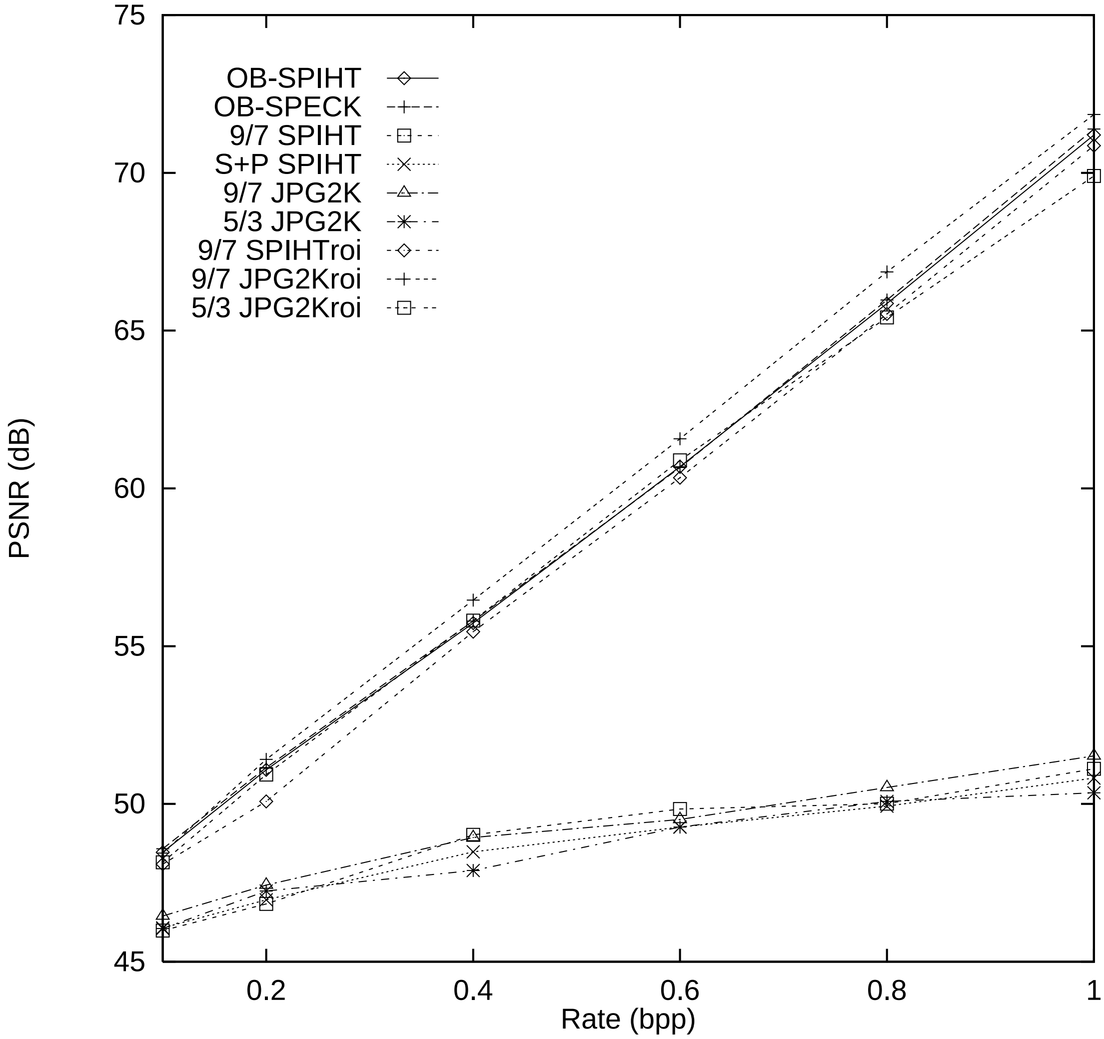

Fig. 7. Comparative evaluation of OB-SPIHT and OB-SPECK with SPIHT and JPEG 2000 for mammogram h56cd.

TABLE I

PSNR (dB) AT VARIOUS RATES FOR MAMMOGRAM h13xd.

Rate (bpp)	OB-SPIHT	OB-SPECK	9/7 SPIHT	S+P SPIHT	9/7 JPG2K	5/3 JPG2K	9/7 SPIHTroi	9/7 JPG2Kroi	5/3 JPG2Kroi
0.1	47.95	48.04	46.64	46.61	47.14	46.70	47.72	48.11	47.88
0.2	50.03	50.08	47.96	48.22	48.67	48.07	49.88	50.43	50.09
0.4	53.41	53.57	50.02	49.88	50.65	49.96	53.19	53.87	53.66
0.6	56.58	56.61	51.37	51.44	52.02	51.75	56.37	57.41	56.79
0.8	60.31	60.24	53.09	53.28	53.69	52.96	60.09	61.29	60.57
1.0	63.74	63.84	54.03	53.89	54.44	54.04	63.39	64.81	64.20

TABLE II

PSNR (dB) AT VARIOUS RATES FOR MAMMOGRAM h44ci.

Rate (bpp)	OB-SPIHT	OB-SPECK	9/7 SPIHT	S+P SPIHT	9/7 JPG2K	5/3 JPG2K	9/7 SPIHTroi	9/7 JPG2Kroi	5/3 JPG2Kroi
0.1	47.90	48.03	46.15	46.27	46.91	46.37	47.59	48.02	47.75
0.2	50.30	50.42	47.69	47.77	48.44	47.64	50.06	50.69	50.29
0.4	54.19	54.30	49.93	49.37	50.07	49.52	53.90	54.68	54.41
0.6	57.78	57.88	50.10	50.31	50.93	50.31	57.47	58.47	58.07
0.8	61.74	61.87	51.49	50.91	52.00	51.07	61.44	62.87	62.11
1.0	66.02	66.14	52.82	53.12	52.99	51.94	65.72	67.37	65.68

TABLE III

PSNR (dB) AT VARIOUS RATES FOR MAMMOGRAM h56cd.

Rate (bpp)	OB-SPIHT	OB-SPECK	9/7 SPIHT	S+P SPIHT	9/7 JPG2K	5/3 JPG2K	9/7 SPIHTroi	9/7 JPG2Kroi	5/3 JPG2Kroi
0.1	48.47	48.58	45.99	46.07	46.45	46.05	48.09	48.44	48.15
0.2	51.08	51.15	46.83	46.96	47.43	47.24	50.80	51.41	50.93
0.4	55.73	55.80	49.02	48.48	48.94	47.89	55.46	56.46	55.81
0.6	60.69	60.66	49.84	49.27	49.51	49.27	60.34	61.57	60.89
0.8	65.86	65.97	50.01	49.93	50.52	50.08	65.53	66.86	65.42
1.0	71.20	71.39	51.11	50.82	51.52	50.35	70.86	71.85	69.90

TABLE IV

PSNR (dB) at various rates for mammogram h58cd.

Rate (bpp)	OB-SPIHT	OB-SPECK	9/7 SPIHT	S+P SPIHT	9/7 JPG2K	5/3 JPG2K	9/7 SPIHTroi	9/7 JPG2Kroi	5/3 JPG2Kroi
0.1	51.33	51.42	48.56	48.46	49.10	48.59	50.86	51.53	51.22
0.2	54.64	54.69	50.54	50.17	50.78	50.38	54.19	54.93	54.67
0.4	60.70	60.64	51.89	51.46	52.31	51.70	60.24	61.46	60.85
0.6	66.97	67.02	53.92	53.62	54.03	52.95	66.41	68.02	66.57
0.8	73.38	73.59	54.63	54.28	54.62	54.13	72.66	74.05	71.87
1.0	80.32	80.72	54.94	55.09	56.00	55.07	78.87	80.29	80.75

TABLE V

PSNR (dB) at various rates for mammogram h60ci.

Rate (bpp)	OB-SPIHT	OB-SPECK	9/7 SPIHT	S+P SPIHT	9/7 JPG2K	5/3 JPG2K	9/7 SPIHTroi	9/7 JPG2Kroi	5/3 JPG2Kroi
0.1	45.45	45.52	44.49	44.64	44.95	44.60	45.20	45.54	45.28
0.2	47.17	47.26	46.02	46.07	46.63	46.25	46.97	47.39	47.10
0.4	49.80	49.88	48.09	48.04	48.41	48.14	49.64	50.27	49.9
0.6	52.00	52.13	49.50	49.09	49.84	49.15	51.82	52.45	52.19
0.8	54.51	54.46	50.39	50.48	51.09	50.56	54.34	55.15	54.88
1.0	56.57	56.61	51.40	51.71	52.26	51.82	56.36	57.47	56.98

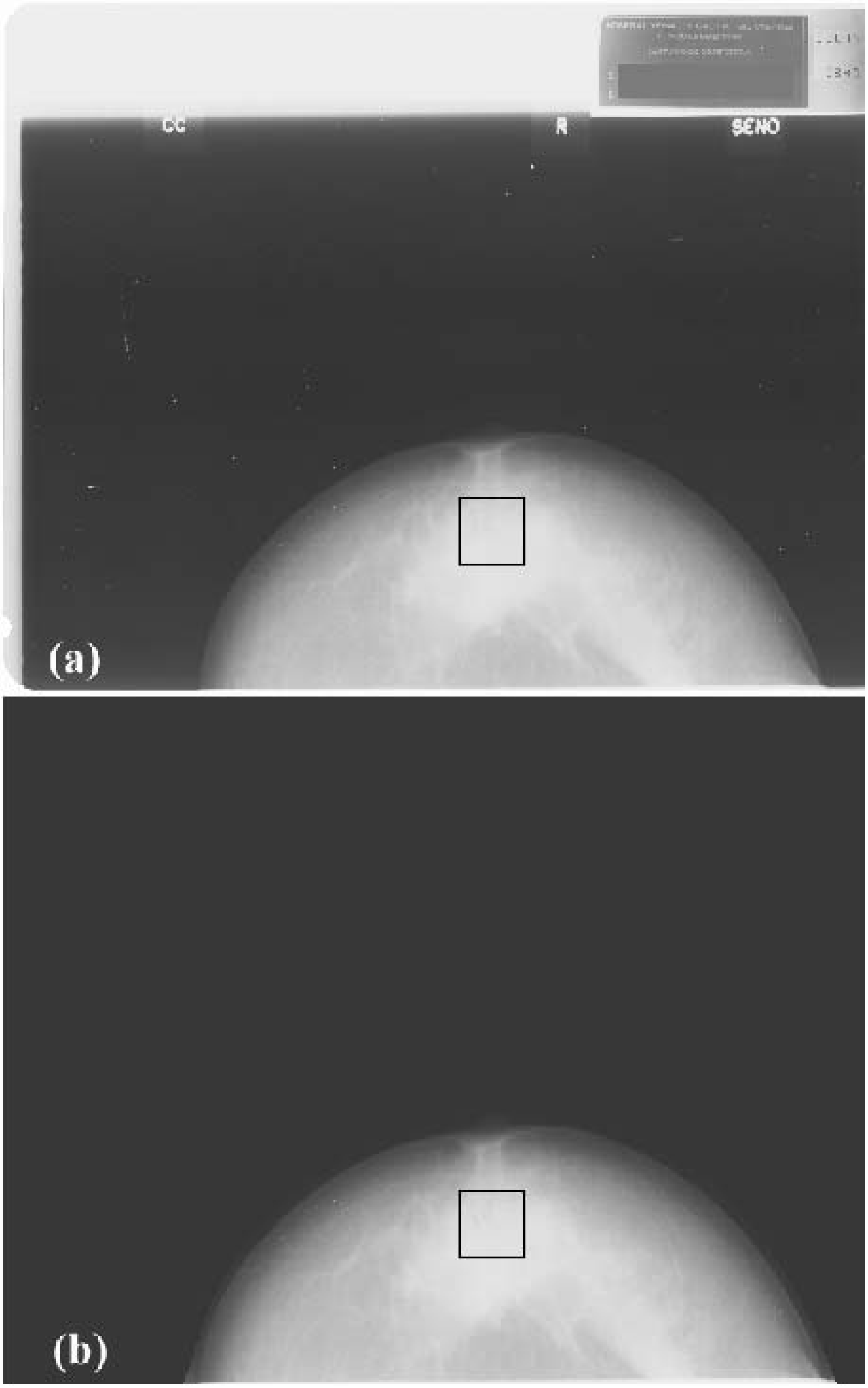

Fig. 8. Reconstructed digital mammogram after compression at 0.4 bpp using: (a) a general compression method as the SPIHT coding algorithm with 9/7 filters, and (b) a region-based method as the OB-SPIHT coding algorithm. Region-based methods improve compression efficiency not coding radiological background.

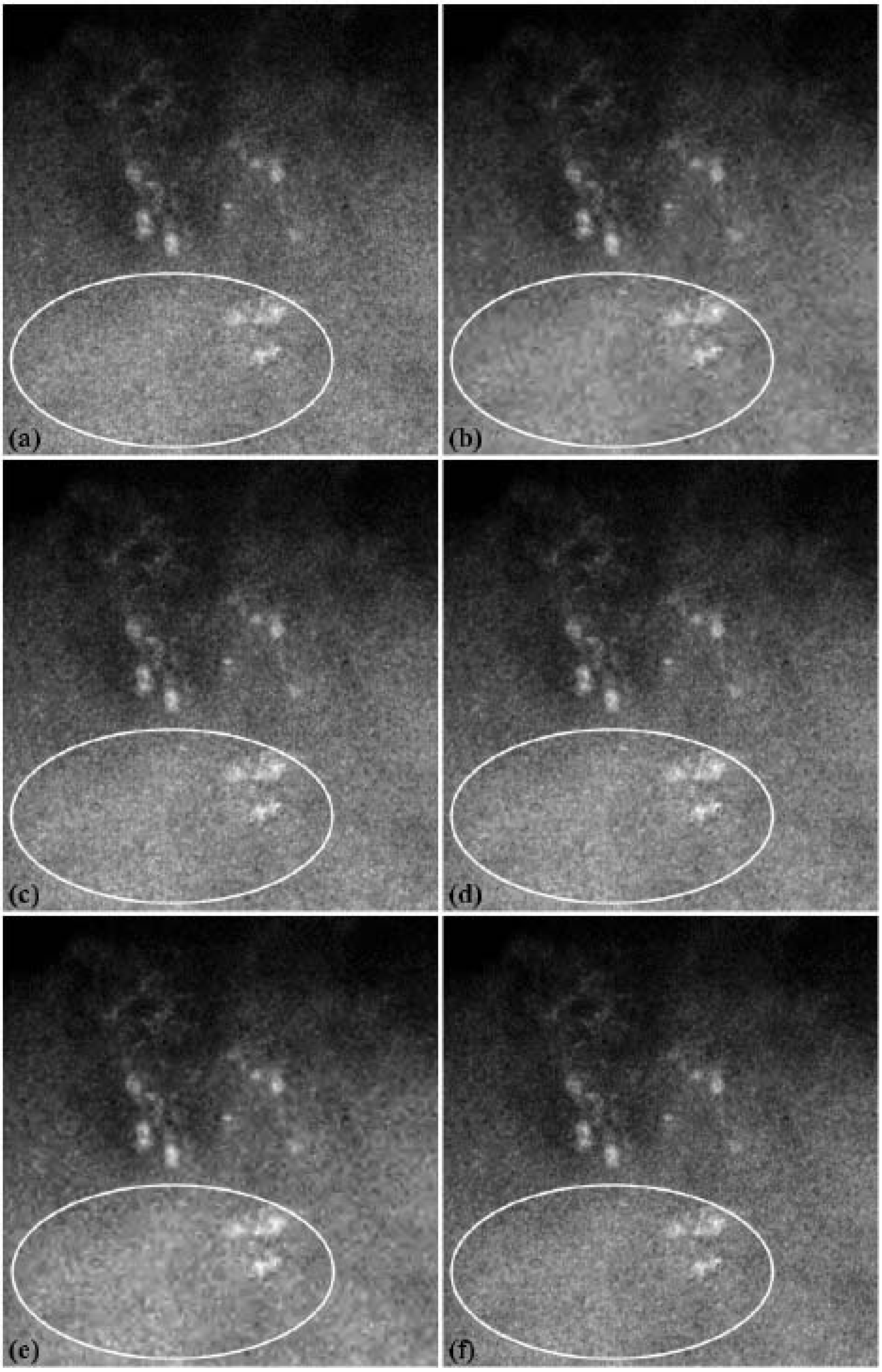

Fig. 9. Region of interest containing a cluster of microcalcifications: (a) in the original image, (b) after 9/7 SPIHT compression at 0.4 bpp, (c) after OB-SPECK compression at 0.4 bpp, (d) after OB-SPIHT compression at 0.4 bpp, (e) after 9/7 JPEG2000 compression at 0.4 bpp, and (f) after 9/7 JPEG2000 compression at 0.4 bpp of the preprocessed image with background set to zero. Rice artifacts are shown with general compression methods (b) and (e).